Charge-switchable ligand ameliorated cobalt polyphthalocyanine polymers for high-current-density electrocatalytic CO_2 reduction

Kong, Xin; Liu, Bin; Tong, Zhongqiu; Bao, Rui; Yi, Jianhong; Bu, Shuyu; Liu, Yunpeng; Wang, Pengfei; Lee, Chun-Sing; Zhang, Wenjun

RESEARCH ARTICLE

SmartMat WILEY

Charge-switchable ligand ameliorated cobalt polyphthalocyanine polymers for high-current-density electrocatalytic CO_2 reduction

Xin Kong[1,2,3] | Bin Liu[1] | Zhongqiu Tong[2,3] | Rui Bao[3] | Jianhong Yi[3] | Shuyu Bu[2] | Yunpeng Liu[4] | Pengfei Wang[5] | Chun-Sing Lee[2,6] | Wenjun Zhang[2,6] (iD)

[1]State Key Laboratory of Chemical Resource Engineering, College of Chemistry, Beijing University of Chemical Technology, Beijing, China

[2]Department of Materials Science and Engineering, Center of Super-Diamond and Advanced Films (COSDAF), City University of Hong Kong, Hong Kong, China

[3]Department of Materials Science and Engineering, Kunming University of Science and Technology, Kunming, China

[4]Institute of High Energy Physics, Chinese Academy of Sciences, Beijing, China

[5]Key Laboratory of Photochemical Conversion and Optoelectronic Materials, Technical Institute of Physics and Chemistry, Chinese Academy of Sciences, Beijing, China

[6]City University of Hong Kong Shenzhen Research Institute, Shenzhen, China

Correspondence
Bin Liu, State Key Laboratory of Chemical Resource Engineering, College of Chemistry, Beijing University of Chemical Technology, Beijing 100029, China.
Email: binliu@buct.edu.cn

Yunpeng Liu, Institute of High Energy Physics, Chinese Academy of Sciences, Beijing 100190, China.
Email: liuyunpeng@ihep.ac.cn

Wenjun Zhang, Department of Materials Science and Engineering, Center of Super-Diamond and Advanced Films (COSDAF), City University of Hong Kong Shenzhen Research Institute, Shenzhen 518000, China.
Email: apwjzh@cityu.edu.hk

Abstract

Metallic phthalocyanines are promising electrocatalysts for CO_2 reduction reaction (CO_2RR). However, their catalytic activity and stability (especially under high potential) are still unsatisfactory. Herein, we synthesized a covalent organic polymer (COP-CoPc) by introducing charge-switchable viologen ligands into cobalt phthalocyanine (CoPc). The COP-CoPc exhibits great activity for CO_2RR, including a high Faradaic efficiency over a wide potential window and the highest CO partial current density among all ligand-tuned phthalocyanine catalysts reported in the H-type cell. Particularly, COP-CoPc also shows great potential for practical applications, for example, a FE_{CO} of >95% is realized at a large current density of $150 \, mA/cm^2$ in a two-electrode membrane electrode assembly reactor. Ex situ and in situ X-ray absorption fine structure spectroscopy measurements and theory calculations reveal that when the charge-switchable viologen ligands switch to neutral-state ones, they can act as electron donors to enrich the electron density of Co centers in COP-CoPc and enhance the desorption of *CO, thus improving the CO selectivity. Moreover, the excellent reversible redox capability of viologen ligands and the increased Co–N bonding strength in the Co–N_4 sites enable COP-CoPc to possess outstanding stability under elevated potentials and

currents, enriching the knowledge of charge-switchable ligands tailored CO_2RR performance.

KEYWORDS

charge-switchable ligand, cobalt phthalocyanine, electrochemical CO_2 reduction reaction, MEA test

1 | INTRODUCTION

The electrochemical reduction of CO_2 is one of the most promising approaches for carbon capture and utilization, in which with CO_2 as the feedstock, high-value-added chemicals and fuels, such as carbon monoxide, methane, methanol, formic acid, and ethanol, can be synthesized at ambient pressure and room temperature. The electrochemical reduction of CO_2 provides an attractive pathway for achieving a sustainable carbon cycle and the goal of carbon neutrality.[1–5] However, electrochemical CO_2 reduction reaction (CO_2RR) suffers from sluggish reaction kinetics due to the chemical inertness of CO_2 molecules and complex reaction pathways with the multielectron transfer. Adding to that, the redox potentials for different CO_2RR products are close to that for hydrogen evolution reaction (HER) in aqueous electrolyte, and the electrocatalytic CO_2RR processes are thus accompanied by competitive HER, which results in low efficiency and poor selectivity of the CO_2 conversion.[6–8] To promote the efficiency of CO_2RR to meet the requirement of practical applications, developing electrocatalysts with high catalytic activity and selectivity, admirable stability, and low cost is essential.

Phthalocyanine-based metal complexes (PcMCs), such as cobalt phthalocyanine (CoPc) and nickel phthalocyanine (NiPc), have been demonstrated to be potential electrocatalysts for CO_2 reduction.[9,10] Compared with other catalysts, such catalysts have well-defined active centers and easily tunable structures, which are favorable for understanding their catalytic mechanisms, thus modulating their catalytic activity and selectivity.[6,11–13] However, in the CO_2RR applications, the PcMCs usually exhibit limited intrinsic activity and poor electrical conductivity, leading to a high overpotential and a low current density. Moreover, their stability is poor under elevated potentials and currents.[14–17] In this context, modifying the metal phthalocyanines with other functional substituents has been revealed to be a promising approach to enhancing their catalytic performance.[14–18] For example, Ren et al.[15] reported that incorporating a nitro or amino ligand next to a single Co atom catalytic center in CoPc could favor or hinder the electrocatalytic CO_2 reduction due to the

respective electron-withdrawing or electron-donating capability of the ligand. Choi et al.[18] immobilized Co (II) phthalocyanine (CoPc-A) onto chemically converted graphene (CCG) via $\pi-\pi$ stacking, and CCG/CoPc-A demonstrated an enhanced catalytic activity as a result of reduced aggregation due to long alkoxy chains. These approaches are able to improve the catalytic activity of CoPc molecules. However, their CO Faradaic efficiency (FE_{CO}) and CO current density (J_{CO}) are still low as compared with other inorganic cobalt-based catalysts. Additionally, undesirable reduction of Pc ligands in reductive conditions deteriorates the long-term stability of PcMCs catalysts, especially under high-overpotential conditions, which is also a fundamental problem to be solved.[20]

In this work, we synthesize a covalent organic polymer by introducing viologen ligands into CoPc (termed COP-CoPc). It has been revealed that viologen has three distinct redox states during reversible redox reactions, that is, dicationic state with positive charges, radical-cationic state, and neutral state,[20] as shown in Figure 1A. When the charge-switchable viologen is introduced in the CoPc molecule, the local electronic environment of the CoPc center will be modulated. Particularly, the viologen in the neutral state has lone pair electrons and extended $\pi-\pi$ conjugation, which enables it to function as an electron donor to enrich the electron density of the Co center (Figure 1B).[16,21] Meanwhile, the delocalization of π electrons in the extended π-π conjugation of COP-CoPc may reduce the negative charges of the ring ligands and thus further increase the electron density of Co centers.[22] Moreover, viologen's excellent reversible redox capability is expected to endow viologen-modified CoPc with good catalytic stability during the CO_2RR process.[22] In the electrochemical CO_2 reduction experiments, the synthesized COP-CoPc exhibits a high FE_{CO} over a wide potential window. Notably, the COP-CoPc also shows a high selectivity and outstanding stability at an elevated current density in a scale-up anion membrane electrode assembly (MEA) reactor. This work demonstrates an effective approach to boost the catalytic activity, selectivity, and stability of CoPc molecules for CO_2RR via charge-switchable ligand modification. It would pave a
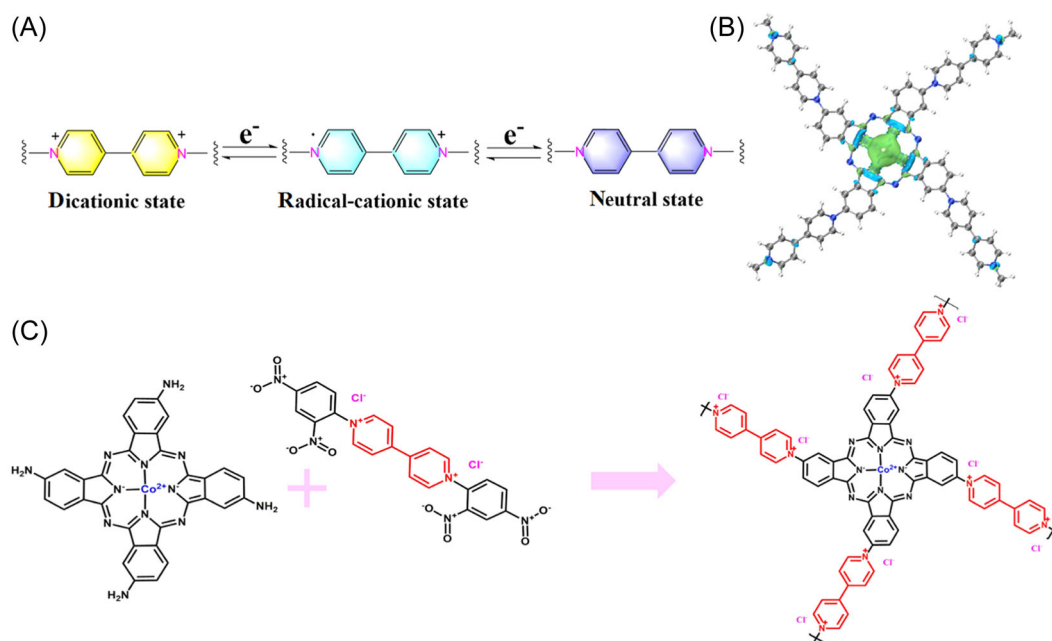
FIGURE 1 (A) Viologen ligands with three distinct redox states during reversible redox reactions: dicationic state, radical-cationic state, and neutral state with lone pair electrons. (B) Top view of the charge density difference of covalent organic polymer (COP-CoPc). The depletion and accumulation spaces of charge are revealed in cyan and green, respectively. (C) Schematic illustration of the synthesis reaction of COP-CoPc.

new avenue for large-scale CO production using molecular electrocatalysts.

2 | RESULTS AND DISCUSSION

2.1 | Synthesis and characterization of COP-CoPc

COP-CoPc was synthesized through a Zincke reaction between an amino derivative of cobalt polyphthalocyanine (CoPc-NH$_2$) and viologen ligands (C$_{22}$H$_{14}$Cl$_2$N$_6$O$_8$), as shown in Figure 1C.[23] The synthesized COP-CoPc is irregularly shaped nanoparticles similar to other control samples of CoPc-NH$_2$ and CoPc, as shown in Supporting Information S1: Figure S1. The EDX mapping images in Supporting Information S1: Figure S2 confirm the homogeneous distributions of C, Co, N, and O in COP-CoPc nanoparticles. The XRD patterns in Supporting Information S1: Figure S3 reveal that in contrast to the crystalline form of CoPc and CoPc-NH$_2$, the synthesized COP-CoPc shows a broad hump at 25–30°, indicating its amorphous nature. To understand the structure of COP-CoPc, the Fourier-transform infrared (FTIR) spectra and Raman spectra of the viologen ligand, CoPc, CoPc-NH$_2$, and COP-CoPc were obtained (Figure 2A,B). For the FTIR spectrum of CoPc-COP, the characteristic absorptions of amino-derivative Pc

macrocycles appear at 3324 and 3204 cm^{-1} (N–H stretching of amino groups), 1609 cm^{-1} (C=C of phenyl rings), and 1488 cm^{-1} (C=N stretching of Pc macrocycles).[17] The characteristic absorptions of viologen ligand at 1549 cm^{-1} is assigned to the –NO$_2$ stretching vibration peak; and this peak disappears in COP-CoPc, which is due to the reaction between –NO$_2$ of viologen and –NH$_2$ of CoPc-NH$_2$ during the formation of COP-CoPc by Zincke reaction (Figure 2A).[17,23,24] In addition, the peaks in the range of 3200–3400 cm^{-1} of COP-CoPc are weaker than those of CoPc-NH$_2$ because of the consumed NH$_2$ groups during the Zincke condensation reaction.[17,25] In the Raman spectrum of COP-CoPc (Figure 2B), a band at 1538 cm^{-1} is observed, which is attributed to the interaction of Co with the phthalocyanine ring and is consistent with those of CoPc and CoPc-NH$_2$. The observation demonstrates that the phthalocyanine structure remains unchanged after the introduction of viologen ligands.[16,19] Moreover, in the UV–Vis spectra of COP-CoPc, CoPc-NH$_2$, and CoPc (Figure 2C), the location of the B band (Soret band, corresponding to the transition from the deeper $a_{2u}(\pi)$ to LUMO.[11,16]) at 300–350 nm and Q band (corresponding to the $a_{1u}(\pi)$–$e_g(\pi^*)$ electron transition from the highest occupied molecular orbital [HOMO] to the lowest unoccupied molecular orbital [LUMO]) at 600–700 nm is different, the Q band of COP-CoPc displays a redshift concerning those of both CoPc-NH$_2$ and CoPc, and the
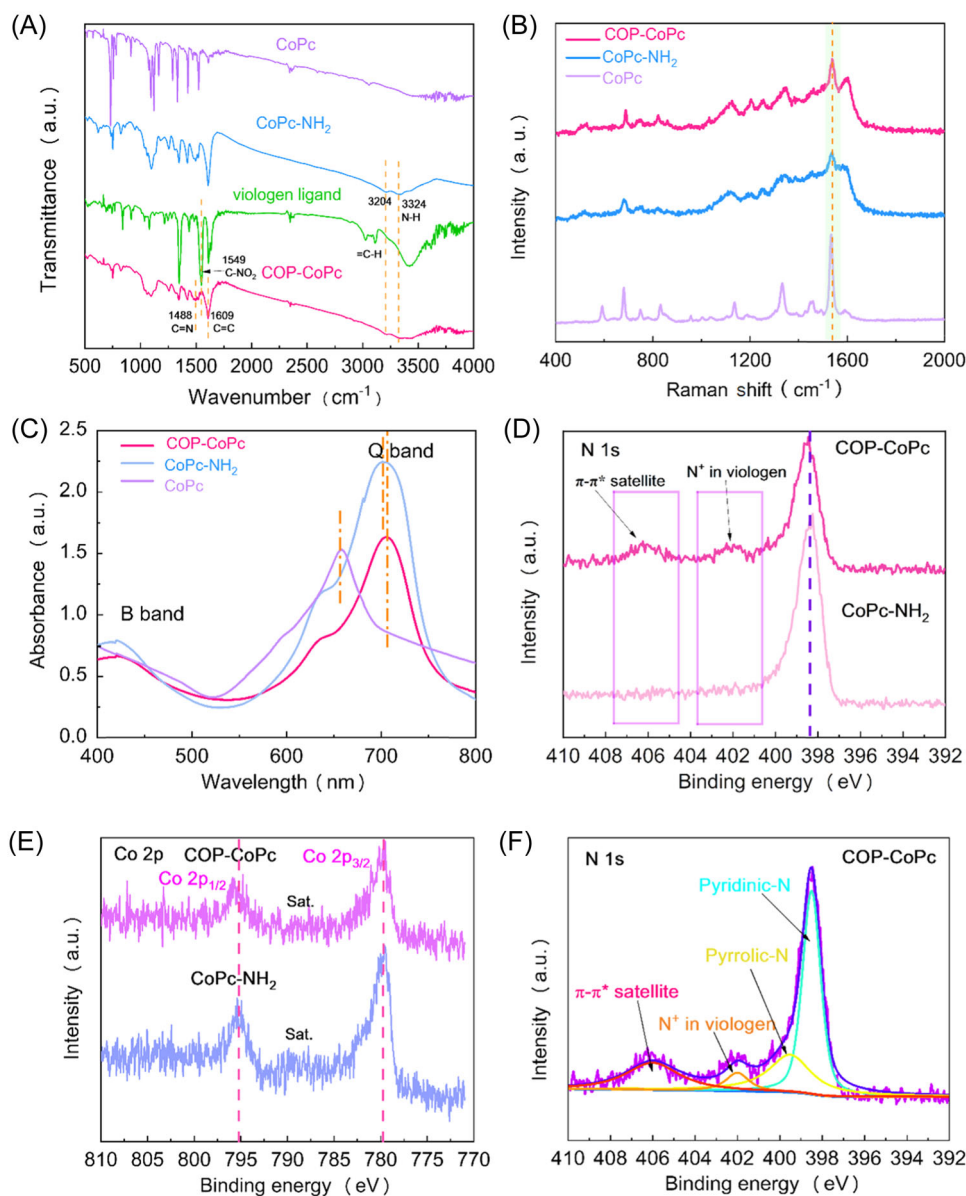
FIGURE 2 (A) Fourier-transform infrared spectra of covalent organic polymer (COP-CoPc), viologen ligand, CoPc-NH₂, and CoPc. (B) Raman spectra of COP-CoPc, CoPc-NH₂, and CoPc. (C) UV-Vis spectra of COP-CoPc, CoPc-NH₂, and CoPc in dimethylformamide (DMF) solutions. High-resolution X-ray photoelectron spectroscopy (XPS) spectra of (D) N 1s and (E) Co 2p of COP-CoPc and CoPc-NH₂, and (F) deconvolution of high-resolution XPS N 1s spectrum of COP-CoPc.

modification of the functional groups resulted in different absorption peak shifts, which suggests the difference of electron states among the samples.[16,17,22]

X-ray photoelectron spectroscopy (XPS) was performed to investigate the surface chemical compositions and states of COP-CoPc. In the high-resolution N 1s XPS spectrum of COP-CoPc (Figure 2D), a significant shift towards a higher binding energy by ~0.3 eV is observed compared to that of CoPc-NH₂. Correspondingly, the Co 2p peak of COP-CoPc also upshifts by ~0.5 eV concerning that of CoPc-NH₂ (Figure 2E). The electron-withdrawing effect of the positive charge of dicationic viologen ligands

causes such deviations in the binding energies of the Co and N peaks.[21] Noticeably, in the deconvoluted high-resolution N 1s XPS spectrum of COP-CoPc (Figure 2F), in addition to the peaks at 398.5 and 399.6 eV for pyridinic and pyrrolic N, respectively,[26,27] the peaks centered at 402.0 and 406.0 eV for the positively charged nitrogen ($-N^+$) in viologen[28–30] and $\pi-\pi^*$ satellite (characteristic signal of nitrogen-containing aromatic polymers[31]), respectively, are also observed, which further verifies the successful synthesis of COP-CoPc.

To further understand the local coordination of COP-CoPc, the Co *K*-edge X-ray absorption near-edge

structure (XANES) spectra of CoPc and COP-CoPc are shown in Figure 3A. It is noted that the absorption edge of COP-CoPc shifts to a higher energy versus that of CoPc, indicating a reduced electron density of Co atoms in COP-CoPc, probably due to the incorporation of dicationic viologen ligands with positive charges. The Fourier transformation (FT) of the extended X-ray absorption fine structure (EXAFS) spectra reveals the coordination environments of Co sites (Figure 3B and Supporting Information S1: Figure S4). The coordination numbers (N) of the first Co−N shell of COP-CoPc and CoPc are calculated to be 3.9 and 3.8 (Supporting Information S1: Table S1), respectively, which are close to the theoretical value of 4, suggesting the similar Co-N coordination structures of the two samples. However, compared with CoPc, the neutral viologen ligands in COP-CoPc serve as electron-donating groups, increasing the electron density around the central cobalt atom, making it more electron-rich. The increased electron density on the cobalt atom enhances its interaction with the nitrogen atoms of the ligand, leading to a reduced Co−N bond length from 1.92 to 1.89 Å (Supporting Information S1: Table S1). Figure 3C,D present the Morlet wavelet transform (WT) contour plots of CoPc and COP-CoPc, in which the intensity maxima are mainly related to the bond length R (R direction) and atomic number Z (k direction). It is noted that the intensity maximum corresponding to the Co−N coordination in COP-CoPc slightly shifts toward smaller $R + \Delta R$ compared to that in CoPc, which is consistent with the altered local environments of the Co sites in the two samples.

2.2 | Influence of functional ligands on the electrocatalytic CO_2RR performance of COP-CoPc

The electrocatalytic CO_2RR performances of COP-CoPc, CoPc-NH_2, and CoPc were evaluated in a CO_2-saturated $KHCO_3$ solution (0.5 mol/L) using a three-electrode H-type cell. As presented in Figure 4A, the linear sweep voltammetry (LSV) curve of COP-CoPc shows better CO_2RR activity as compared with CoPc-NH_2 and CoPc. The gas reduction products were detected to be dominantly CO and H_2 at the investigated potentials by using gas chromatography (GC). The FEs_{CO} of these three samples under different potentials are shown in Figure 4B. Among them, the COP-CoPc delivers a maximum FE_{CO} of 97.3% at −0.88 V versus reversible hydrogen electrode (RHE), superior to CoPc-NH_2 (89.0%) and CoPc (87.3%). Such a high FE_{CO} empowers COP-CoPc to outperform most of the phthalocyanine-based COP catalysts reported thus far, such as the
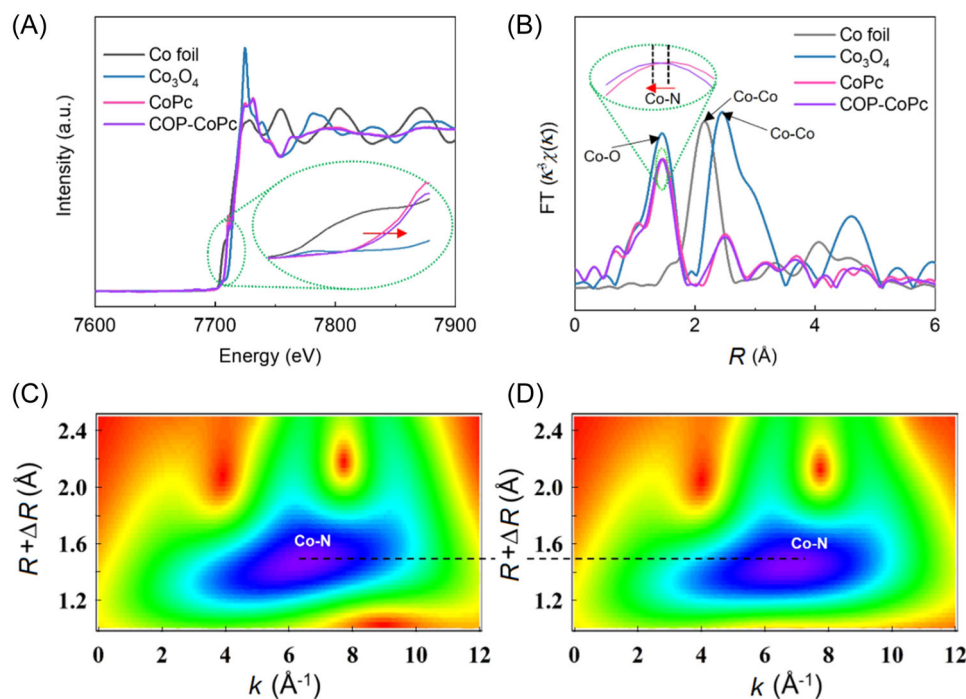

FIGURE 3 (A) Co K-edge X-ray absorption near-edge structure spectra of CoPc and covalent organic polymer (COP-CoPc), and (B) the corresponding Fourier transforms of Co K-edge extended X-ray absorption fine structure spectra, wavelet transform contour plots of k^3-weighted $\chi(k)$ signals of (C) CoPc and (D) COP-CoPc.
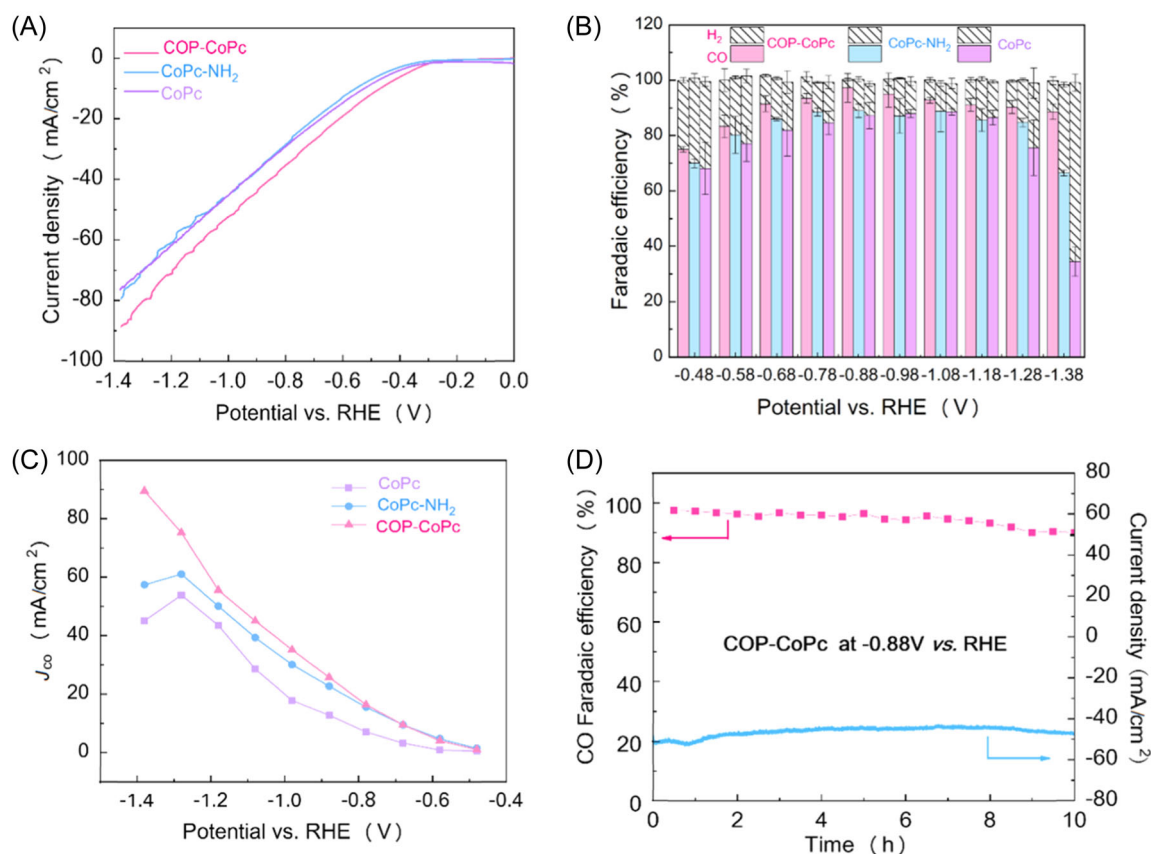
FIGURE 4 (A) Linear sweep voltammetry curves of COP-CoPc, CoPc-NH$_2$, and CoPc. (B) FE$_S$ of CO and H$_2$ for all samples at various potentials. (C) J_{CO} of samples at various potentials. (D) Long-term stability of COP-CoPc at −0.88 V versus RHE. RHE, reversible hydrogen electrode.

CoPc-imidazole (FE$_{CO}$ = 71% at −1.25 V vs. SCE),[14] amino-CoPc/G (FE$_{CO}$ = 67.5% at −0.88 V vs. RHE),[15] squaraine-bridged cobalt tetraamino phthalocyanine COP-SA (FE$_{CO}$ = 96.5% at 0.65 V vs. RHE), and 1,4-benzenedicarboxaldehyde-bridged cobalt tetraamino phthalocyanine BDA (FE$_{CO}$ = 85% at −0.65 V vs. RHE).[17] Particularly, COP-CoPc maintains a high FE$_{CO}$ (>90%) over a wide potential range from −0.68 to −1.28 V versus RHE. As references, CoPc-NH$_2$ and CoPc have severe hydrogen evolution at increased potentials and thus dramatically decreased FE$_{CO}$, for example, 64.5% and 34.5% at −1.28 V for CoPc-NH$_2$ and CoPc, respectively. The above results demonstrate the superior selectivity of COP-CoPc in CO$_2$RR, which is attributed to the incorporation of a charge-switchable viologen ligand that induces electron localization of Co sites, as verified by the DFT analysis below.[16]

According to the chronoamperometric responses of COP-CoPc, CoPc-NH$_2$, and CoPc (Supporting Information S1: Figure S5–S7), their CO partial current densities (J_{CO}) were calculated, as depicted in Figure 4C. Notably, COP-CoPc delivers much enlarged J_{CO} than the control samples, in particular at elevated potentials, for example,

90 mA/cm^2 for COP-CoPc versus 45 mA/cm^2 for CoPc and 57 mA/cm^2 for CoPC-NH$_2$ at −1.4 V versus RHE. It is also worth noting that this current density is the highest among all ligand-tuned phthalocyanine molecule catalysts reported for the CO$_2$RR in the H-type cell. Together with the extraordinarily high FE$_{CO}$, COP-CoPc is one of the best electrocatalysts for CO$_2$RR reported thus far, as shown in Supporting Information S1: Table S2.[14–17,19] To further evaluate the intrinsic activity of the catalysts, the TOFs$_{CO}$ of the samples are calculated as shown in Supporting Information S1: Figure S8. It is revealed that COP-CoPc has a TOF$_{CO}$ of 0.67 s^{-1}, which is much larger than that of CoPc-NH$_2$ (0.19 s^{-1}) and CoPc (0.13 s^{-1}), indicating the superior intrinsic activity of COP-CoPc for CO$_2$RR. Apart from activity, the long-term durability of the COP-CoPc catalyst for CO$_2$RR was also investigated. As shown in Figure 4D, the J_{CO} remains almost stable, and the FE$_{CO}$ of COP-CoPc maintains within the range of 97.6%–91.6% for 10 h electrolysis at −0.88 V versus RHE, suggesting that COP-CoPc has outstanding stability. To evaluate the durability of COP-CoPc, the STEM-HAADF images of COP-CoPc before and after electrocatalysis are performed in Supporting Information S1: Figure S9. The

result indicates that COP-CoPc maintains its pristine structure, and no metal clusters are observed after the stability test.

2.3 | Insight into the CO₂RR process on COP-CoPc catalyst with in situ/operando XAS characterization and DFT calculations

We performed the in situ XAS to probe the valence states of COP-CoPc under real electrocatalytic CO₂RR conditions. As is shown in Figure 5A, in comparison with that at open-circuit voltage (OCV), no significant change is detected in the in situ XANES Co K-edge spectra of COP-CoPc at −0.1 V versus RHE, indicating that COP-CoPc remains unchanged under such a potential, that is, CO₂RR is not catalyzed by COP-CoPc. When the potential is elevated to −0.4 and −0.6 V, the absorption edge shifts increasingly toward lower energy, suggesting a partial reduction of the Co centers in COP-CoPc. Correspondingly, the current density increases from null at OCV or −0.1 V to 1.2 mA/cm² in the LSV curve (Figure 4A). Based on the above results and previous reports, a possible electrocatalytic pathway for the CO₂RR on COP-CoPc is proposed, as illustrated in
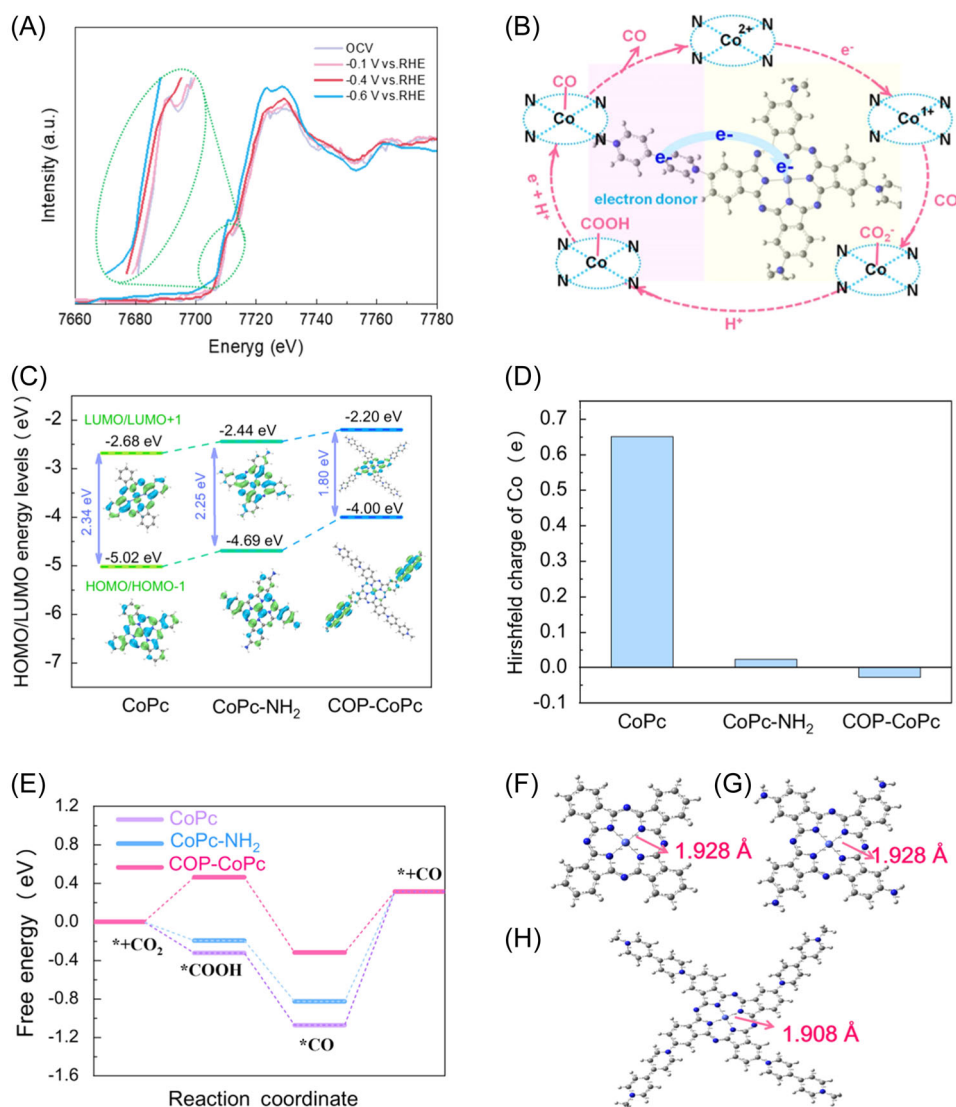

FIGURE 5 (A) Normalized in situ cobalt K-edge X-ray absorption near-edge structure spectra of CoP-CoPc at open-circuit voltage, −0.1, −0.4, −0.6 V versus RHE in CO₂-saturated 0.5 mol/L KHCO₃. (B) Schematic diagram showing the electrocatalytic pathways for CO₂RR on covalent organic polymer (COP-CoPc). (C) Calculated energy levels and electron density distributions of alpha-doubly degenerate HOMO/ HOMO − 1 and LUMO/LUMO + 1 of CoPc, CoPc-NH₂ and COP-CoPc. (D) The Hirshfeld charge of Co sites in CoPc, CoPc-NH₂, and COP-CoPc. (E) Free energy variations for the reaction steps in the reduction of CO₂ to CO on CoPc, CoPc-NH₂, and COP-CoPc. The Co–N bond length in (F) CoPc, (G) CoPc-NH₂, and (H) COP-CoPc. RHE, reversible hydrogen electrode.

Figure 5B. First, the Co^{2+} centers are reduced to a lower-valence state, for example, $Co^{\delta+}$ ($\delta < 2$) under the assistance of an external bias, and CO_2 molecules are adsorbed on the Co^+ sites and reduced to $*CO_2^-$, accompanied by the oxidation of $Co^{\delta+}$. Then, $*COOH$ is formed due to hydrogenation of $*CO_2^-$. Finally, $*COOH$ is converted to $*CO$ via the second proton-coupled electron transfer process, followed by the desorption of CO molecules from the Co centers on COP-CoPc.[32]

Density functional theory (DFT) calculations were performed to elucidate the origin of the excellent CO_2RR activity of COP-CoPc. Under the condition of electro-catalytic CO_2RR, dicationic viologen will be reduced to neutral-state viologen.[21] As a result, the neutral-state viologen ligands were used to construct the DFT model of COP-CoPc. Alpha-doubly degenerated HOMO/HOMO − 1 and LUMO/LUMO + 1 electron density distributions and energy levels were derived, as shown in Figure 5C. It is revealed that CoPc-NH_2 and CoPc have similar electronic structures. However, with the incorporation of neutral-state viologen ligands, the electron density distributions of the highest occupied molecular orbital (HOMO/HOMO − 1) and lowest unoccupied molecular orbital (LUMO/LUMO + 1) of COP-CoPc change significantly. Specifically, the HOMO electrons of COP-CoPc are mainly located on the neutral-state viologen ligands, while the LUMO electrons are mainly gathered around the Co centers (Figure 5C). The calculations suggest that the electrons of neutral-state viologen ligands are transferred to the Co centers, which leads to more electrons located at the Co sites and makes them catalytically more active.[32] These results are consistent with the Hirshfeld population analysis, which also reveals the creation of electron-rich cobalt environments in COP-CoPc compared to those in CoPc and CoPc-NH_2 (Figure 5D). In addition, the HOMO energy level of COP-CoPc upshifts from −5.02 eV of CoPc to −4.00 eV due to the incorporation of stronger electron-donating neutral-state viologen ligands, which endows COP-CoPc with enhanced reducibility.[3] Meanwhile, COP-CoPc has a much smaller energy gap between LUMO and HOMO (1.80 eV) in comparison with CoPc (2.34 eV) and CoPc-NH_2 (2.25 eV), which facilitates the electron transport in COP-CoPc during the CO_2RR progress.[33] The similar variation of beta-doubly degenerated LUMO/HOMO energy levels is also observed due to the introduction of viologen ligands in COP-CoPc (Supporting Information S1: Figure S10).

Gibbs free energy changes (ΔG) of the reactions were calculated according to the reaction pathway at different sites (The schematic configurations of the adsorbed species on the surfaces of CoPc, CoPc-NH_2, and COP-CoPc during CO_2RR are presented in Supporting

Information S1: Figure S11). The free energy variations for the reaction steps during the reduction of CO_2 to CO on CoPc, CoPc-NH_2, and COP-CoPc are shown in Figure 5E. It is revealed that the $*CO$ desorption on the active Co centers is the rate-determining step. The ΔG for the release of adsorbed CO is 0.76 eV on COP-CoPc, which is lower than those on CoPc-NH_2 (1.14 eV) and on CoPc (1.38 eV). The results indicate that $*CO$ species are more easily desorbed on COP-CoPc, and thus, more active sites are exposed for the subsequent reactions. Furthermore, considering that HER is a competing reaction in CO_2RR, the free energy diagrams of HER were calculated. It is revealed that COP-CoPc has a high positive free energy change for adsorbed hydrogen intermediates during HER (Supporting Information S1: Figure S12), which is conducive to HER suppression. This agrees well with the experimental observations of its excellent selectivity towards CO_2RR (a high FE_{CO} over a wide potential). More importantly, as shown in Figure 5F–H, the Co–N bond length is calculated to be 1.909 Å in COP-CoPc, being smaller than those of CoPc-NH_2 (1.928 Å) and CoPc (1.928 Å). The shortened Co–N bond length induced by the neutral-state viologen ligands enhances the bond strength of Co–N_4 sites. As a result, the severe deactivation of CoPc caused by Co–N bond breakage during irreversible Co(II)/Co(I) redox at high potentials can be effectively reduced, and the stability of COP-CoPc electrocatalyst under high potentials is enhanced.[34,35]

2.4 | Two-electrode MEA tests of the CO_2RR performance of COP-CoPc

The MEA device was further adopted to test the CO_2RR performance of COP-CoPc at large current density. The schematic diagram of the MEA system is shown in Figure 6A, and the valid areas of both cathodes loaded with COP-CoPc and anode loaded with IrO_2 are 5 cm^2. The electrolyte of 0.5 mol/L $KHCO_3$ was used to minimize the effect of possible salt accumulation at high current densities. Figure 6B presents the FE_{CO} of COP-CoPc at different current densities. A high FE_{CO} over 95% is achieved even at a high current density of 150 mA/cm^2. Moreover, the stability test was also conducted without flushing the electrode or refreshing the electrolyte to evaluate the durability of the device without mainte-nance. As shown in the time-dependent voltage curve at a constant current of 0.25 A (Figure 6C), the COP-CoPc assembled MEA retains a high FE_{CO} of over 90% for no less than 48 h with a slight increase of full-cell voltage from 2.7 to 2.9 V. Note that the electrodes were not flushed and the electrolyte was not refreshed during the
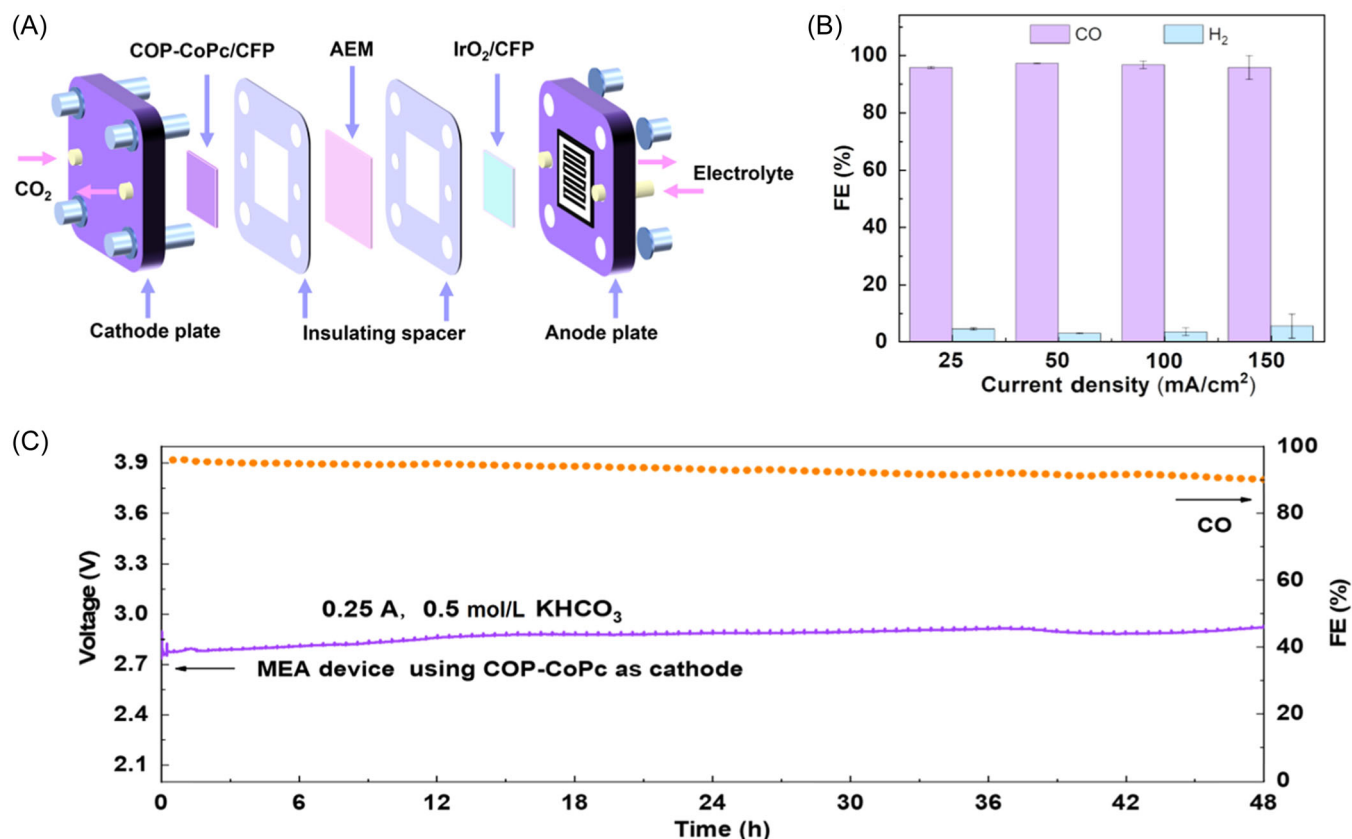
FIGURE 6 (A) Schematic diagram of the 5 cm² membrane electrode assembly (MEA) reactor. (B) FE_{CO} of covalent organic polymer (COP-CoPc) assembled MEA in 0.5 mol/L $KHCO_3$ electrolyte at various current densities. (C) Time-dependent voltage and FE_{CO} of COP-CoPc assembled MEA device at a current of 0.25 A in 0.5 mol/L $KHCO_3$ electrolyte.

test, which highlights the excellent stability of COP-CoPc for future practical applications.

3 | CONCLUSION

In summary, we have designed and synthesized COP-CoPc for CO_2 electroreduction to CO using the charge-switchable viologen ligands to ameliorate CoPc. The COP-CoPc exhibits a superior CO_2RR performance, for example, a high FE_{CO} (>90%) over a wide potential window (–0.68 to –1.28 V), a maximum FE_{CO} of 97.3% at –0.88 V versus RHE, and a large current density of 101 mA/cm² at –1.38 V versus RHE in an H-type setup, which makes it the best among all developed ligand-tuned phthalocyanine molecule catalysts for CO_2RR, and as well as one of the best electrocatalysts for CO_2RR reported thus far. Impressively, COP-CoPc also demonstrates its potential for practical applications, for example, a FE_{CO} of over 95% is realized at a large current density of 150 mA/cm² in a 5 cm² scale-up MEA system. The neutral-state viologen ligands in situ formed during CO_2RR are illustrated to enrich the

electron density of single-atom Co sites in COP-CoPc and enhance the desorption of *CO intermediates, leading to an increased catalytic activity of COP-CoPc for CO_2RR. Moreover, the excellent reversible redox capability of viologen ligands and the strong Co–N bonding strength in the $Co-N_4$ sites enable COP-CoPc to possess outstanding stability under elevated potentials and currents. Incorporating charge-switchable ligand coordination to modulate the activity and stability of CoPc-based electrocatalysts may provide a useful approach for designing highly active MePc-based electrocatalysts for industrial CO_2RR applications.

CONFLICT OF INTEREST STATEMENT
The authors declare no conflicts of interest.

DATA AVAILABILITY STATEMENT

The data that support the findings of this study are available from the corresponding author upon reasonable request.

ORCID

Wenjun Zhang http://orcid.org/0000-0002-4497-0688

REFERENCES

1. Li F, Thevenon A, Rosas-Hernández A, et al. Molecular tuning of CO_2-to-ethylene conversion. *Nature*. 2020;577(7791): 509-513.
2. Angamuthu R, Byers P, Lutz M, Spek AL, Bouwman E. Electrocatalytic CO_2 conversion to oxalate by a copper complex. *Science*. 2010;327(5963):313-315.
3. Zhang X, Wang Y, Gu M, et al. Molecular engineering of dispersed nickel phthalocyanines on carbon nanotubes for selective CO_2 reduction. *Nat Energy*. 2020;5(9):684-692.
4. Reddu V, Sun L, Li X, Jin H, Wang S, Wang X. Highly selective and efficient electroreduction of CO_2 in water by quaterpyridine derivative-based molecular catalyst noncovalently tethered to carbon nanotubes. *SmartMat*. 2022;3(1):151-162.
5. Zheng S-J, Cheng H, Yu J, et al. Three-dimensional ordered porous N-doped carbon-supported accessible Ni-N_x active sites for efficient CO_2 electroreduction. *Rare Met*. 2023;42(6): 1800-1807.
6. Birdja YY, Pérez-Gallent E, Figueiredo MC, Göttle AJ, Calle-Vallejo F, Koper MTM. Advances and challenges in understanding the electrocatalytic conversion of carbon dioxide to fuels. *Nat Energy*. 2019;4(9):732-745.
7. Vasileff A, Zheng Y, Qiao SZ. Carbon solving carbon's problems: recent progress of nanostructured carbon-based catalysts for the electrochemical reduction of CO_2. *Adv Energy Mater*. 2017;7(21):1700759.
8. Liu Y, Wu T, Cheng H, Wu J, Guo X, Fan HJ. Active plane modulation of Bi_2O_3 nanosheets via Zn substitution for efficient electrocatalytic CO_2 reduction to formic acid. *Nano Res*. 2023;16(8):10803-10809.
9. Mao J, Mei B, Li J, et al. Unraveling the dynamic structural evolution of phthalocyanine catalysts during CO_2 electroreduction. *Chinese J Struc Chem*. 2022;41(10):2210082-2210088.
10. Wan C-P, Yi J-D, Cao R, Huang Y-B. Conductive metal/covalent organic frameworks for CO_2 electro-reduction. *Chinese J Struc Chem*. 2022;41(5):2205001-2205014.
11. Han N, Wang Y, Ma L, et al. Supported cobalt polyphthalocyanine for high-performance electrocatalytic CO_2 reduction. *Chem*. 2017;3(4):652-664.
12. Zhang Y, Rawat RS, Fan HJ. Plasma for rapid conversion reactions and surface modification of electrode materials. *Small Methods*. 2017;1(9):1700164.
13. Chen Y, Wang L, Yao Z, et al. Tuning the coordination structure of single atoms and their interaction with the support for carbon dioxide electroreduction. *Acta Physico Chimica Sinica*. 2022;38(11):2207024-2207044.
14. Rivera Cruz KE, Liu Y, Soucy TL, Zimmerman PM, McCrory CCL. Increasing the CO_2 reduction activity of cobalt phthalocyanine by modulating the σ-donor strength of axially coordinating ligands. *ACS Catal*. 2021;11(21):13203-13216.
15. Ren X, Liu S, Li H, et al. Electron-withdrawing functional ligand promotes CO_2 reduction catalysis in single atom catalyst. *Sci China Chem*. 2020;63(12):1727-1733.
16. Chen K, Cao M, Lin Y, et al. Ligand engineering in nickel phthalocyanine to boost the electrocatalytic reduction of CO_2. *Adv Funct Mater*. 2022;32(10):2111322.
17. Song Y, Zhang J-J, Zhu Z, et al. Zwitterionic ultrathin covalent organic polymers for high-performance electrocatalytic carbon dioxide reduction. *Appl Catal B*. 2021;284(5):119750.
18. Jiang Z, Zhang Z, Li H, et al. Molecular catalyst with near 100% selectivity for CO_2 reduction in acidic electrolytes. *Adv Energy Mater*. 2023;13(6):2203603.
19. Choi J, Wagner P, Gambhir S, et al. Steric modification of a cobalt phthalocyanine/graphene catalyst to give enhanced and stable electrochemical CO_2 reduction to CO. *ACS Energy Lett*. 2019;4(3):666-672.
20. Wu Y, Jiang Z, Lu X, Liang Y, Wang H. Domino electroreduction of CO_2 to methanol on a molecular catalyst. *Nature*. 2019;575(7784):639-642.
21. Liu X, Neoh KG, Kang ET. Viologen-functionalized conductive surfaces: physicochemical and electrochemical characteristics, and stability. *Langmuir*. 2002;18(23):9041-9047.
22. Chen K, Cao M, Ni G, et al. Nickel polyphthalocyanine with electronic localization at the nickel site for enhanced CO_2 reduction reaction. *Appl Catal B*. 2022;306(7):121093.
23. Skorjanc T, Shetty D, Gándara F, et al. Remarkably efficient removal of toxic bromate from drinking water with a porphyrin–viologen covalent organic framework. *Chem Sci*. 2020;11(3):845-850.
24. Zhang X, Liu H, An P, et al. Delocalized electron effect on single metal sites in ultrathin conjugated microporous polymer nanosheets for boosting CO_2 cycloaddition. *Sci Adv*. 2020;6(17):eaaz4824.
25. Ding X, Han B-H. Metallophthalocyanine-based conjugated microporous polymers as highly efficient photosensitizers for singlet oxygen generation. *Angew Chem Int Ed*. 2015;54(22): 6536-6539.
26. Cao L, Fang G, Wang Y. Electroreduction of viologen phenyl diazonium salts as a strategy to control viologen coverage on electrodes. *Langmuir*. 2017;33(4):980-987.
27. Kong X, Liu G, Peng H-Q, et al. Plasma-induced transformation: a new strategy to in situ engineer MOF-derived heterointerface for high-efficiency electrochemical hydrogen evolution. *J Mater Chem A*. 2022;10(12):6596-6606.
28. Liu X. Enzymatic activity of glucose oxidase covalently wired via viologen to electrically conductive polypyrrole films. *Biosens Bioelectron*. 2004;19(8):823-834.
29. Feng R, Chen Y, Yang L, Du Q, Zhuo K. Ethyl viologen-functionalized reduced graphene oxide composites for asymmetric ionic liquid-based supercapacitors. *Chem Eng J*. 2023;468(7):143693.
30. Wang L, Ding J, Sun S, et al. Viologen-hypercrosslinked ionic porous polymer films as active layers for electronic and energy storage devices. *Adv Mater Interfaces*. 2018;5(10):1701679.
31. Rignanese GM, Pasquarello A, Charlier JC, Gonze X, Car R. Nitrogen incorporation at Si (001)-SiO_2 interfaces: relation between N 1s core-level shifts and microscopic structure. *Phys Rev Lett*. 1997;79(25):5174-5177.

32. Wang T, Guo L, Pei H, et al. Electron-rich pincer ligand-coupled cobalt porphyrin polymer with single-atom sites for efficient (photo)electrocatalytic CO_2 reduction at ultralow overpotential. *Small.* 2021;17(45):2102957.

33. Wang H, Wang H, Si Z, et al. A bipolar and self-polymerized phthalocyanine complex for fast and tunable energy storage in dual-ion batteries. *Angew Chem Int Ed.* 2019;58(30):10204-10208.

34. Woodward AN, Kolesar JM, Hall SR, Saleh N-A, Jones DS, Walter MG. Thiazolothiazole fluorophores exhibiting strong fluorescence and viologen-like reversible electrochromism. *J Am Chem Soc.* 2017;139(25):8467-8473.

35. Das G, Prakasam T, Nuryyeva S, et al. Multifunctional redox-tuned viologen-based covalent organic polymers. *J Mater Chem A.* 2016;4(40):15361-15369.

SUPPORTING INFORMATION

Additional supporting information can be found online in the Supporting Information section at the end of this article.